

Lifshitz transition and frustration of magnetic moments in infinite-layer NdNiO₂ upon hole-doping

I. Leonov,^{1,2} S. L. Skornyakov,^{1,2} and S. Y. Savrasov³

¹*M.N. Miheev Institute of Metal Physics, Russian Academy of Sciences, 620108 Yekaterinburg, Russia*

²*Ural Federal University, 620002 Yekaterinburg, Russia*

³*University of California, Davis*

Motivated by the recent discovery of superconductivity in the infinite-layer (Sr,Nd)NiO₂ films with Sr content $x \simeq 0.2$ [Li et al., *Nature (London)* **572**, 624 (2019)], we examine the effects of electron correlations and Sr-doping on the electronic structure, Fermi surface topology, and magnetic correlations in (Nd,Sr)NiO₂ using a combination of dynamical mean-field theory of correlated electrons and band-structure methods. Our results reveal a remarkable orbital selective renormalization of the Ni 3d bands, with $m^*/m \sim 3$ and 1.3 for the $d_{x^2-y^2}$ and $d_{3z^2-r^2}$ orbitals, respectively, that suggests orbital-dependent localization of the Ni 3d states. We find that upon hole doping (Nd,Sr)NiO₂ undergoes a Lifshitz transition of the Fermi surface which is accompanied by a change of magnetic correlations from the three-dimensional (3D) Néel *G*-type (111) to the quasi-2D *C*-type (110). We show that magnetic interactions in (Nd,Sr)NiO₂ demonstrate an unanticipated frustration, which suppresses magnetic order, implying the importance of in-plane spin fluctuations to explain its superconductivity. Our results suggest that frustration is maximal for Sr-doping $x \simeq 0.1-0.2$, which is in agreement with an experimentally observed doping value Sr $x \simeq 0.2$ of superconducting (Nd,Sr)NiO₂.

The recent discovery of superconductivity in the infinite-layer Sr-doped NdNiO₂ films (Nd_{0.8}Sr_{0.2}NiO₂) with the critical temperature up to $T_c \sim 15$ K has attracted a lot of attention from researchers around the world [1]. NdNiO₂ has a similar planar crystal structure to that of the parent “infinite layer” superconductor CaCuO₂, which exhibits superconductivity below $T_c \simeq 110$ K upon hole doping [2–4]. As Ni is isoelectronic to copper in NdNiO₂, it has a nominal d^9 configuration. Based on this, it was expected that analogous to cuprates the low energy physics of Sr-doped NdNiO₂ is dominated by electrons in the planar Ni x^2-y^2 states. However, unlike cuprates, in the infinite-layer nickelate the Ni x^2-y^2 states are found to experience strong hybridization with the Nd 5d orbitals (primarily the $3z^2-r^2$ and xy orbitals), yielding a non-cuprate-like Fermi surface [5, 6]. While the electronic structure of NdNiO₂ has recently been widely studied using various band structure methods [7–9], model techniques [10, 11], and DFT+dynamical mean-field theory (DFT+DMFT) [12, 13] methods [14–19], the properties of Sr-doped NdNiO₂ are still poorly understood. For NdNiO₂, DFT+DMFT calculations reveal significant correlation effects within the Ni 3d orbitals, which are complicated by large hybridization with the Nd 5d states [14, 18]. Moreover, based on the experiments two features that are central to copper oxides – the ZhangRice singlet and large planar spin fluctuations – were claimed to be absent (or diminished) in (Nd,Sr)NiO₂ [1, 6].

Here we explore the effects of electronic correlations and Sr-doping on the electronic structure of (Nd,Sr)NiO₂ using a fully self-consistent in charge density DFT+DMFT method [12, 13] implemented with plane-wave pseudopotentials [20, 21]. DFT+DMFT has been proved to be among the most advanced theoretical methods for studying the electronic properties of

strongly correlated materials, such as correlated transition metal oxides, heavy-fermions, Fe-based superconductors, e.g., to study the phenomena of a Mott transition, collapse of local moments, large orbital-dependent renormalizations, etc. [22] We use this advanced computational method to study the Fermi surface topology and magnetic correlations, as well as their impact on magnetism of (Nd,Sr)NiO₂ upon Sr-doping.

We adopt the experimental lattice parameters measured for the Nd_{0.8}Sr_{0.2}NiO₂ film grown on the SrTiO₃ substrate (space group $P4/mmm$, lattice parameters $a = 3.91$ Å and $c = 3.37$ Å) [1]. Following the literature, to avoid the numerical instabilities arising from the Nd 4f electrons we focus on La³⁺ instead of Nd³⁺ ($4f^3$) ion [8, 11, 15]. (Hereafter, we assume La by saying Nd in our calculations). To explore the effect of Sr-doping on the electronic structure of (Nd,Sr)NiO₂ we employ a rigid-band shift of the Fermi level within DFT. In our DFT+DMFT calculations we explicitly include the Ni 3d, Nd 5d, and O 2p valence states, by constructing a basis set of atomic-centered Wannier functions within the energy window spanned by these bands [23]. This allows us to take into account a charge transfer between the partially occupied Ni 3d, Nd 5d, and O 2p states, accompanied by the strong on-site Coulomb correlations of the Ni 3d electrons. We use the continuous-time hybridization expansion (segment) quantum Monte Carlo algorithm in order to solve the realistic many-body problem [24]. We take the average Hubbard $U = 6$ eV and Hund’s exchange $J = 0.95$ eV as previously employed for rare-earth nickelates R NiO₃ [25]. We use the fully localized double-counting correction, evaluated from the self-consistently determined local occupations, to account for the electronic interactions already described by DFT.

In Fig. 1 we display our results for the \mathbf{k} -resolved spectra of paramagnetic (PM) (Nd,Sr)NiO₂ obtained by

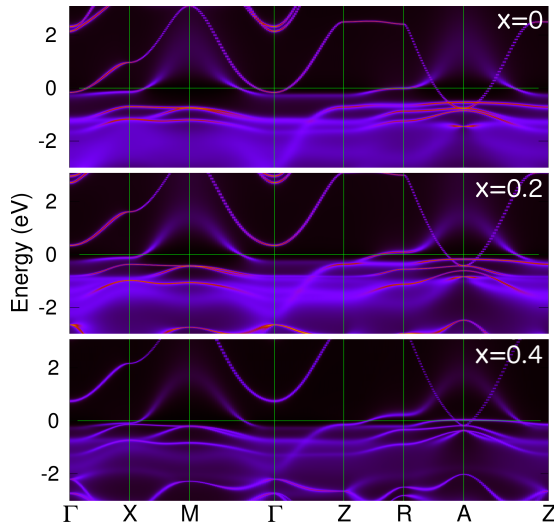


FIG. 1: k -resolved spectral function of Sr-doped NdNiO₂ for Sr $x = 0$ (top), $x = 0.2$ (middle) and $x = 0.4$ (bottom) as obtained by DFT+DMFT for the paramagnetic state at $T = 290$ K.

DFT+DMFT as a function of Sr doping x . Overall, our results agree well with those published previously [11, 15, 18]. For Sr $x = 0$ we observe a band formed by the strongly mixed Ni and Nd $3z^2 - r^2$ states crossing the Fermi level near the Γ point. Upon Sr x (hole) doping these states are seen to shift above the Fermi level, resulting in a change of the electronic structure of (Nd,Sr)NiO₂.

Our DFT+DMFT calculations reveal a remarkable orbital-selective renormalization of the partially occupied Ni $x^2 - y^2$ and $3z^2 - r^2$ bands (shown in Fig. 2). In particular, for Sr $x = 0$ the Ni $x^2 - y^2$ states exhibit a large mass renormalization of $m^*/m \sim 3$, while correlation effects in the $3z^2 - r^2$ band are significantly weaker, $m^*/m \sim 1.3$. This behavior is consistent with sufficiently different occupations of the Ni $x^2 - y^2$ and $3z^2 - r^2$ orbitals. In fact, the $x^2 - y^2$ orbital occupancy for Sr $x = 0$ is close to half-filling (~ 0.58 per spin-orbital), while the $3z^2 - r^2$ orbitals are nearly fully occupied (~ 0.84). In addition, our analysis of the local spin susceptibility $\chi(\tau) = \langle \hat{m}_z(\tau) \hat{m}_z(0) \rangle$ (see Fig. S1) suggests the proximity of the Ni $x^2 - y^2$ states to localization, while the Ni $3z^2 - r^2$ electrons are delocalized. Indeed, $\chi(\tau)$ for the Ni $3z^2 - r^2$ states is seen to decay fast to zero with the imaginary time τ , which is typical for itinerant behavior. In contrast to that $\chi(\tau)$ for the $x^2 - y^2$ states is sufficiently larger, $\chi(0) = 0.72 \mu_B^2$, slowly decaying to $\sim 0.07 \mu_B^2$ at $\tau = \beta/2$. Our results therefore suggest that magnetic correlations in NdNiO₂ are at the verge of orbital-dependent formation of local magnetic moments [14]. In agreement with this the calculated (instantaneous) magnetic moment of Ni is about $\sqrt{\langle \hat{m}_z^2 \rangle} \simeq 1.1 \mu_B$, which is consistent with nearly a $S = 1/2$ state of nickel.

Upon hole doping the Ni $3d$ occupations slightly decrease to 0.52 and 0.80 (per spin-orbital) for the Ni $x^2 - y^2$

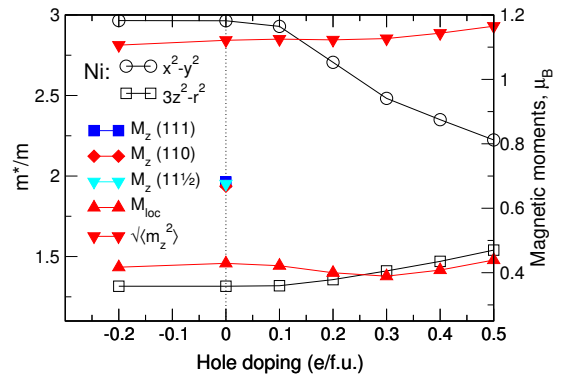


FIG. 2: Orbitaly resolved quasiparticle mass enhancement m^*/m together with the instantaneous $\sqrt{\langle \hat{m}_z^2 \rangle}$ and fluctuating magnetic moments $M_{\text{loc}} = [T \int_0^{1/T} \langle \hat{m}_z(\tau) \hat{m}_z(0) \rangle]^{1/2}$ of Sr-doped NdNiO₂ calculated by DFT+DMFT for the paramagnetic state, at $T = 290$ K. M_z : DFT+DMFT results for magnetization per Ni site for the Néel (111), C -type (110), and $(11\frac{1}{2})$ AFM states at $T = 290$ K.

and $3z^2 - r^2$ orbitals, respectively, for Sr $x = 0.5$. This corresponds to a ~ 0.17 decrease of the total Wannier Ni $3d$ occupation, whereas the Nd $5d$ and O $2p$ states occupancies drop by ~ 0.21 and 0.06 . In addition, we observe a gradual decrease of mass renormalization of the $x^2 - y^2$ states to $m^*/m \sim 2.3$ at Sr $x = 0.5$. In contrast to that for the $3z^2 - r^2$ orbital m^*/m slightly increases to ~ 1.5 . We notice no qualitative change in the self-energy upon changing of the Sr content x . The Ni $3d$ states obey a Fermi-liquid-like behavior with a weak damping at the Fermi energy. Moreover, doping with Sr does not affect much magnetic moments in the paramagnetic phase of (Nd,Sr)NiO₂. Thus, the instantaneous magnetic moments $\sqrt{\langle \hat{m}_z^2 \rangle}$ tend to increase only by about 5%. Interestingly in our model calculations (with absent self-consistency over the charge density, i.e., for the fixed tight-binding parameters of the DFT Wannier Hamiltonian) this increase is more significant, about 63%, suggesting the proximity to spin freezing, in accordance to recent model DMFT calculations [14].

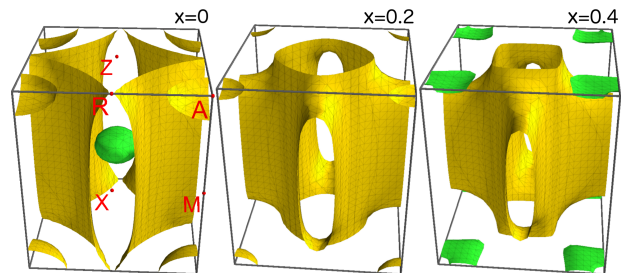


FIG. 3: Quasiparticle Fermi surface of Sr-doped NdNiO₂ for Sr $x = 0, 0.2,$ and 0.4 calculated by DFT+DMFT for the paramagnetic state at $T = 290$ K.

Next, we calculate the quasiparticle Fermi surface (FS) of PM NdNiO₂ within DFT+DMFT. In Fig. 3 we show

the dependence of the calculated FS's as a function of Sr x . We note that our results for $x = 0$ are in qualitative agreement with previous band-structure studies [5, 7]. In particular, we obtain that the FS consists of three FS sheets, with the elliptical FS centered at the Brillouin zone (BZ) center (Γ point), originating from the mixed Ni $3d$ and Nd $3z^2 - r^2$ states. The electron FS pockets centered at the A -point are mainly of the Ni xz/yz character. Similar to the cuprates, the FS of NdNiO₂ is dominated by the quasi-two-dimensional (quasi-2D) holelike FS sheet with a predominant Ni $x^2 - y^2$ character, centered at the A - M BZ edge. In close similarity to the cuprates, our results for the FS topology imply an in-plane nesting with magnetic vector $q_m = (110)$ (M -point).

Upon increase of the Sr content, we observe a remarkable change of the electronic structure of (Nd,Sr)NiO₂ which is associated with an entire reconstruction of the FS topology, i.e., a Lifshitz transition. Thus, at $x = 0.2$ the elliptical FS centered at the Γ point vanishes. In addition, the holelike quasi-2D FS sheets at the top and the bottom of the BZ merge near the R point to a quasi-3D electron-like FS that forms a neck at the top and the bottom of the BZ. Overall, this suggests that the Lifshitz transition is accompanied by a reconstruction of magnetic correlations in infinite-layer (Nd,Sr)NiO₂ that appears near to the experimentally observed doping Sr $x \simeq 0.2$.

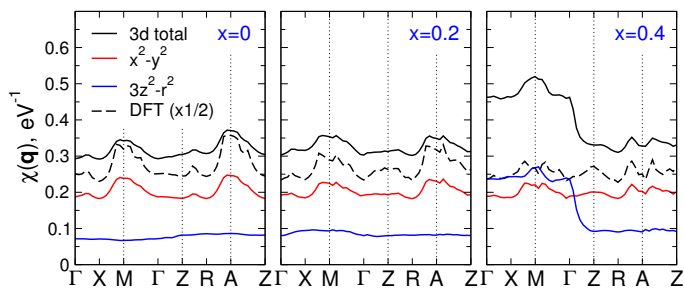


FIG. 4: Orbitally resolved static spin susceptibility $\chi(\mathbf{q})$ of Sr-doped NdNiO₂ calculated by DFT+DMFT at $T = 290$ K.

We proceed with analysis of the symmetry and strength of magnetic correlations in (Nd,Sr)NiO₂. For this purpose we compute the momentum-dependent static magnetic susceptibility $\chi(\mathbf{q})$ within DFT+DMFT using the particle-hole bubble approximation. Orbital contributions of $\chi(\mathbf{q})$ along the BZ path and their dependence on the Sr content x are shown in Fig. 4. Our results for the total $\chi(\mathbf{q})$ as a function of Sr doping x are summarized in Fig. S2. Interestingly for $x = 0$ our results for $\chi(\mathbf{q})$ exhibit two well defined maxima at the M and A points of the tetragonal BZ. This suggests the existence of (at least) two leading magnetic instabilities due to the Ni $x^2 - y^2$ states (for $x = 0$) with a wave vector near to $q_m = (110)$ and (111) , that corresponds to the C -type and the Néel AFM ordering, respectively. In the same time $\chi(\mathbf{q})$ for the $3z^2 - r^2$ states is seen to be small and nearly \mathbf{q} -independent. We notice that $\chi(\mathbf{q})$

appears to be somewhat larger in the A than that in the M point. We therefore expect that the three-dimensional Néel AFM state is more energetically favorable than the quasi-2D C -type (for Sr $x = 0$). In fact, this qualitative analysis agrees well with our total-energy calculations within the spin-polarized DFT and DFT+DMFT methods (see Fig. S3). Both reveal that for Sr $x = 0$ the Néel AFM ordering is more energetically favorable by about 3-4 meV/f.u. with respect to the C -type AFM and the PM state within DFT+DMFT, at $T = 290$ K. We note that within DFT the Néel and the staggered dimer ($11\frac{1}{2}$) and C -type (110) states are differ by about 5-7 meV/f.u., while the non-magnetic state appears much above, by about 85 meV/f.u.

Our results for $\chi(\mathbf{q})$ and total energies suggest that various types of spin order are competing (nearly energetically degenerate) in (Nd,Sr)NiO₂. Indeed, for Sr $x = 0.2$, $\chi(\mathbf{q})$ is seen to be nearly flat and degenerate at around the M and A points (see Fig. 4), implying possible frustration of the Ni $3d$ moments. Upon further increase of Sr x , our results provide a clear evidence of an entire reconstruction of magnetic correlations, with the $3z^2 - r^2$ states now playing a major role. While for Sr $x = 0.4$ $\chi(\mathbf{q})$ for the $x^2 - y^2$ orbital is seen to be nearly flat (degenerate for different \mathbf{q}), suggesting in-plane frustration of the Ni $3d$ moments. The out-of-plane $3z^2 - r^2$ orbital contribution reveals a flat maximum near the M point.

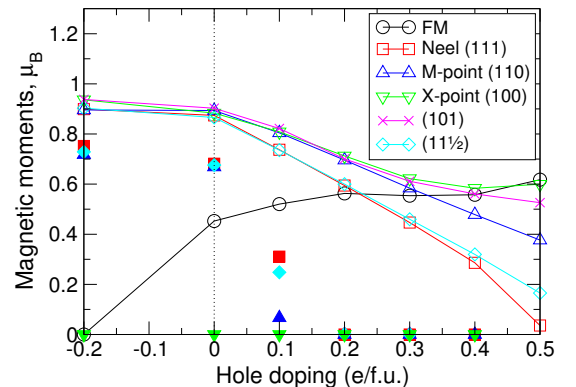


FIG. 5: Long-range ordered magnetic moments of Ni as a function of hole doping calculated for NdNiO₂ by DFT (empty symbols). DFT+DMFT results for the Néel, C -type (110), single stripe (100), and staggered dimer ($11\frac{1}{2}$) AFM states at $T = 290$ K are shown by filled symbols.

In Fig. 5 we show our results for the long-range ordered magnetic moments of nickel calculated within the spin-polarized DFT and DFT+DMFT. The latter are about $0.67 \mu_B/\text{Ni}$ as obtained by DFT+DMFT for the Néel (111), C -type (110), and staggered dimer ($11\frac{1}{2}$) AFM states for Sr $x = 0$, at $T = 290$ K. Notably, we observe a sharp suppression of the calculated magnetization M_z and hence of the Néel temperature evaluated from the spin-polarized DFT+DMFT calculations with Sr x . In particular, for Sr $x = 0.2$ we find no evidence for a mag-

netically ordered state at $T \geq 290$ K. Thus, all magnetic configurations discussed here, namely, the (100), (110), (111) and $(11\frac{1}{2})$ AFM and FM configurations collapse in the PM state. That is, for Sr $x = 0.2$ the Néel (Curie) temperature is much below the room temperature that suggests rising of quantum spin fluctuations with x .

We note, however, that analysis of the finite-temperature DFT+DMFT results may often be problematic. For example, the single stripe (100) AFM and ferromagnetic orderings are found to be unstable at $T = 290$ K, i.e., both collapse to the PM state. We therefore first perform the spin-polarized DFT calculations of the ground state energy differences between different magnetic states (see Fig. S3). In fact, the DFT calculations give qualitatively similar results to those obtained by DFT+DMFT with significantly larger values of the total energy difference (with respect to the non-magnetic state) of ~ 85 meV/f.u., and 8 meV/f.u. for the C -type, Néel, and staggered dimer $(11\frac{1}{2})$, and single stripe (100) magnetic states, respectively. Both spin-polarized DFT and DFT+DMFT calculations reveal a near degeneracy of various types of spin orders, implying frustration of magnetic correlations in (Nd,Sr)NiO₂. The latter is most notable for the Sr content of about $x \simeq 0.2$ – 0.3 , which is close to the experimental Sr doping $x \simeq 0.2$. Moreover, the calculated magnetization for the various AFM states tends to decrease in both the DFT and DFT+DMFT calculations upon increase of Sr x (see Fig. 5). In addition, within DFT+DMFT magnetization is found to sharply collapse to the PM state for Sr $x > 0.1$ at $T = 290$ K, suggesting a sharp increase of spin fluctuations with x .

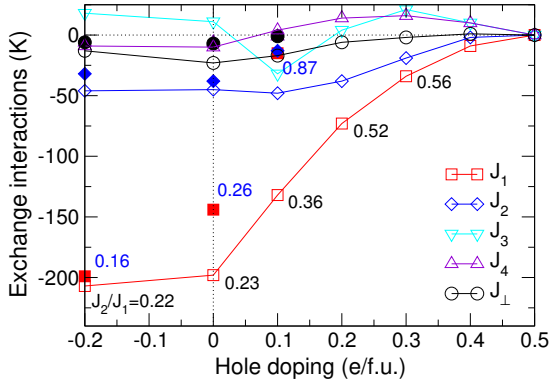


FIG. 6: Exchange interaction parameters (in-plane nearest-neighbor (NN) J_1 , next-nearest neighbor J_2 , 3-rd NN J_3 , 4-th NN J_4 and interlayer coupling J_\perp) of Sr-doped NdNiO₂ calculated within spin-polarized DFT (empty symbols) and DFT+DMFT (filled symbols).

Our results point out an anomalous sensitivity of the electronic structure and magnetic correlations of (Nd,Sr)NiO₂ with respect to the Sr x doping. In particular, we found a remarkable frustration of (orbital-dependent) magnetic moments of Ni sites near to the optimal Sr doping $x \simeq 0.2$. To help check these results, we computed magnetic exchange couplings within the spin-

polarized DFT and DFT+DMFT using the magnetic force theorem [26]. Our findings for the Néel AFM state are summarized in Fig. 6. We observe that for Sr $x = 0$ the interlayer couplings J_\perp is small and weakly antiferromagnetic, $J_\perp \sim -23$ K [27]. The in-plane couplings J_1 (nearest-neighbor) and J_2 (next-nearest-neighbor) are both antiferromagnetic and are sufficiently higher by modulus, ~ 198 K and -45 K, respectively. Interestingly that for pure NdNiO₂, $|J_1| = 198$ K is comparable to that found experimentally in infinite-layer CaCuO₂ [3]. Most importantly, our results reveal a remarkable change of the J_2/J_1 ratio with respect to Sr x , which is increasing from ~ 0.36 to 0.56 for $x = 0.1$ – 0.3 , i.e., near to the experimental doping Sr $x \simeq 0.2$. While in DFT+DMFT magnetization is found to quickly collapse to the PM state for Sr $x > 0.1$, the exchange couplings evaluated from the spin-polarized DFT+DMFT calculations do follow the same trend, with $J_2/J_1 \simeq 0.26$ for Sr $x = 0$, which is found to increase to 0.87 for Sr $x = 0.1$.

Our findings resemble us the behavior of the spin-1/2 frustrated J_1 - J_2 Heisenberg model on the two-dimensional (2D) square lattice, with an unusual quantum spin liquid ground state to appear in the highly frustrated region $J_2/J_1 \simeq 0.4$ – 0.5 , sandwiched between the Néel and stripe type (or valence-bond solid) ordered states [28]. This analogy is very striking, taking into account our results for the change of the electronic structure and magnetic couplings J_2/J_1 ratio in (Nd,Sr)NiO₂ with Sr x . Thus, the frustration region is sandwiched between the two different (long- or short-range ordered) antiferromagnets [28]. We find that magnetic couplings in (Nd,Sr)NiO₂ near to the optimal doping demonstrate an unanticipated frustration, which suppresses a long-range magnetic order (resulting in a drastic drop of the Néel temperature), and can lead to formation of unusual quantum spin liquid ground states. Moreover, our results suggest that frustration is maximal for Sr-doping $x = 0.1$ – 0.2 that corresponds to the highly frustrated region of the spin-1/2 frustrated J_1 - J_2 Heisenberg model. Overall, our results suggest the importance of in-plane spin fluctuations to explain superconductivity in (Nd,Sr)NiO₂, in contrast to the previous claims [1]. We point out that strong frustration of magnetic interactions in (Nd,Sr)NiO₂ suggests that superconductivity in infinite-layer (Nd,Sr)NiO₂ appears to be similar to that observed in iron chalcogenides and pnictides [29].

In conclusion, we employed the DFT+DMFT computational approach to study the effects of electronic correlations and Sr-doping on the electronic structure and magnetic properties of (Nd,Sr)NiO₂. We show that upon hole doping it undergoes a Lifshitz transition of the Fermi surface which is accompanied by a reconstruction of magnetic correlations. Most importantly, magnetic interactions in (Nd,Sr)NiO₂ are found to demonstrate an unanticipated frustration. We find that frustration is maximal for Sr-doping $x = 0.1$ – 0.2 that nearly corresponds to the experimentally observed doping value of (Nd,Sr)NiO₂. Our results for (Nd,Sr)NiO₂ reveal a fea-

ture that is central to copper oxides as well as to iron chalcogenides and pnictides – large in-plane spin fluctuations. We propose that superconductivity in nickelates is strongly influenced, or even induced, by in-plane spin fluctuations.

Acknowledgments

We acknowledge support by the state assignment of Minobrnauki of Russia (theme “Electron” No. AAAA-

A18-118020190098-5). Theoretical analysis of the electronic structure and Fermi surface topology was supported by Russian Foundation for Basic Research (Project No. 18-32-20076). S.Y.S. was supported by National Science Foundation DMR Grant No. 1832728.

-
- [1] D. Li, K. Lee, B. Y. Wang, M. Osada, S. Crossley *et al.*, *Nature (London)* **572**, 624 (2019).
- [2] M. Azuma, Z. Hiroi, M. Takano, Y. Bando, and Y. Takeda, *Nature (London)* **356**, 775 (1992).
- [3] Y. Y. Peng, G. Dellea, M. Minola, M. Conni, A. Amorese *et al.*, *Nat. Phys.* **13**, 1201 (2017).
- [4] S. Y. Savrasov and O. K. Andersen, *Phys. Rev. Lett.* **77**, 4430 (1996).
- [5] V. I. Anisimov, D. Bukhvalov, T. M. Rice, *Phys. Rev. B* **59**, 7901 (1999); K.-W. Lee and W. E. Pickett, *Phys. Rev. B* **70**, 165109 (2004); M.-Y. Choi, K.-W. Lee, and W. E. Pickett, *Phys. Rev. B* **101**, 020503(R) (2020).
- [6] M. Hepting *et al.*, *Nat. Mater.* <https://doi.org/10.1038/s41563-019-0585-z> (2020).
- [7] P. Jiang, L. Si, Z. Liao, and Z. Zhong, *Phys. Rev. B* **100**, 201106 (2019); Y. Nomura, M. Hirayama, T. Tadano, Y. Yoshimoto, K. Nakamura, and R. Arita, *Phys. Rev. B* **100**, 205138 (2019); M. Jiang, M. Berciu, and G. A. Sawatzky, arXiv: 1909.02557 (2019); J. Gao, Z. Wang, C. Fang, and H. Weng, arXiv: 1909.04657 (2019); H. Zhang, L. Jin, S. Wang, B. Xi, X. Shi, F. Ye, and J.-W. Mei, arXiv: 1909.07427 (2019); E. Been, W.-S. Lee, H. Y. Hwang, Y. Cui, J. Zaanen *et al.*, arXiv:2002.12300 (2020).
- [8] A. S. Botana and M. R. Norman, *Phys. Rev. X* **10**, 011024 (2020);
- [9] B. Geisler and R. Pentcheva, arXiv: 2001.03762
- [10] G.-M. Zhang, Y.-F. Yang, and F.-C. Zhang, *Phys. Rev. B* **101**, 020501(R) (2020); X. Wu, D. Di Sante, T. Schwemmer, W. Hanke, H. Y. Hwang, S. Raghu, and R. Thomale, arXiv: 1909.03015 (2019).
- [11] H. Sakakibara, H. Usui, K. Suzuki, T. Kotani, H. Aoki, and K. Kuroki, arXiv: 1909.00060 (2019).
- [12] A. Georges, G. Kotliar, W. Krauth, and M. J. Rozenberg, *Rev. Mod. Phys.* **68**, 13 (1996); G. Kotliar, S. Y. Savrasov, K. Haule, V. S. Oudovenko, O. Parcollet, and C. A. Marianetti, *Rev. Mod. Phys.* **78**, 865 (2006).
- [13] K. Haule, *Phys. Rev. B* **75**, 155113 (2007); L. V. Pourovskii, B. Amadon, S. Biermann, and A. Georges, *Phys. Rev. B* **76**, 235101 (2007); B. Amadon, F. Lechermann, A. Georges, F. Jollet, T. O. Wehling, and A. I. Lichtenstein, *Phys. Rev. B* **77**, 205112 (2008); M. Aichhorn, L. Pourovskii, V. Vildosola, M. Ferrero, O. Parcollet *et al.*, *Phys. Rev. B* **80**, 085101 (2009); I. Leonov, L. Pourovskii, A. Georges, and I. A. Abrikosov, *Phys. Rev. B* **94**, 155135 (2016).
- [14] Ph. Werner and S. Hoshino, *Phys. Rev. B* **101**, 041104(R) (2020).
- [15] S. Ryee, H. Yoon, T. J. Kim, M. Y. Jeong, and M. J. Han, arXiv: 1909.05824 (2019).
- [16] Y. Gu, S. Zhu, X. Wang, J. Hu, and H. Chen, arXiv: 1911.00814 (2019).
- [17] L. Si, W. Xiao, J. Kaufmann, J. M. Tomczak, Y. Lu, Z. Zhong, and K. Held, arXiv: 1911.06917 (2019); M. Kitatani, L. Si, O. Janson, R. Arita, Z. Zhong, K. Held, arXiv: 2002.12230 (2020).
- [18] F. Lechermann, arXiv: 1911.11521 (2019).
- [19] J. Karp, A. S. Botana, M. R. Norman, H. Park, M. Zingl, A. Millis, arXiv: 2001.06441 (2020).
- [20] P. Giannozzi, S. Baroni, N. Bonini, M. Calandra, R. Car *et al.*, *J. Phys.: Condens. Matter* **21**, 395502 (2009).
- [21] I. Leonov, N. Binggeli, Dm. Korotin, V. I. Anisimov, N. Stojić, and D. Vollhardt, *Phys. Rev. Lett.* **101**, 096405 (2008); I. Leonov, Dm. Korotin, N. Binggeli, V. I. Anisimov, and D. Vollhardt, *Phys. Rev. B* **81**, 075109 (2010).
- [22] Z. P. Yin, K. Haule, and G. Kotliar, *Nat. Mater.* **10**, 932 (2011); *Nat. Phys.* **7**, 294 (2011); L. de’ Medici, J. Mravlje, and A. Georges, *Phys. Rev. Lett.* **107**, 256401 (2011); P. Werner, M. Casula, T. Miyake, F. Aryasetiawan, A. J. Millis, and S. Biermann, *Nat. Phys.* **8**, 331 (2012); I. Leonov, S. L. Skornyakov, V. I. Anisimov, and D. Vollhardt, *Phys. Rev. Lett.* **115**, 106402 (2015); S. L. Skornyakov, V. I. Anisimov, D. Vollhardt, and I. Leonov, *Phys. Rev. B* **96** 035137 (2017); P. V. Arribi and L. de’ Medici, *Phys. Rev. Lett.* **121**, 197001 (2018); E. Greenberg, I. Leonov, S. Layek, Z. Konopkova, M. P. Pasternak *et al.*, *Phys. Rev. X* **8**, 031059 (2018); I. Leonov, G.K. Rozenberg, I.A. Abrikosov, *npj Comput. Mater.* **5**, 90 (2019); X. Deng, K. M. Stadler, K. Haule, A. Weichselbaum, J. von Delft, and G. Kotliar, *Nat. Commun.* **10**, 2721 (2019).
- [23] N. Marzari, A. A. Mostofi, J. R. Yates, I. Souza, and D. Vanderbilt, *Rev. Mod. Phys.* **84**, 1419 (2012); V. I. Anisimov, D. E. Kondakov, A. V. Kozhevnikov, I. A. Nekrasov, Z. V. Pchelkina *et al.*, *Phys. Rev. B* **71**, 125119 (2005).
- [24] E. Gull, A. J. Millis, A. I. Lichtenstein, A. N. Rubtsov, M. Troyer, and P. Werner, *Rev. Mod. Phys.* **83**, 349 (2011).
- [25] H. Park, A. J. Millis, and C. A. Marianetti, *Phys. Rev. B* **89**, 245133 (2014); E. A. Nowadnick, J. P. Ruf, H. Park, P. D. C. King, D. G. Schlom *et al.*, *Phys. Rev. B* **92**, 245109 (2015); I. Leonov, A. S. Belozеров, and S. L. Skornyakov, *Phys. Rev. B* **100**, 161112(R) (2019)
- [26] A. I. Liechtenstein, M. I. Katsnelson, V. P. Antropov, and

V. A. Gubanov, J. Magn. Magn. Mater. **67**, 65 (1987); Y. O. Kvashnin, O. Grånäs, I. Di Marco, M. I. Katsnelson, A. I. Lichtenstein, and O. Eriksson, Phys. Rev. B **91**, 125133 (2015).

- [27] Here we adopt the following notation for the Heisenberg model $H = -\sum_{ij} J_{ij} e_i e_j$ where $e_{i,j}$ are the unit vectors.
- [28] S.-S. Gong, W. Zhu, D. N. Sheng, O. I. Motrunich, and M. P. A. Fisher, Phys. Rev. Lett. **113**, 027201 (2014); S. Morita, R. Kaneko, and M. Imada, J. Phys. Soc. Jpn. **84**, 024720 (2015); L. Wang and A. W. Sandvik, Phys. Rev. Lett. **121**, 107202 (2018).
- [29] Q. Si and E. Abrahams, Phys. Rev. Lett. **101**, 076401 (2008); C. Fang, H. Yao, W.-F. Tsai, J. P. Hu, and S. A. Kivelson, Phys. Rev. B **77**, 224509 (2008); C. Xu, M. Müller, and S. Sachdev, Phys. Rev. B **78**, 020501(R) (2008); M. J. Han, Q. Yin, W. E. Pickett, and S. Y. Savrasov, Phys. Rev. Lett. **102**, 107003 (2009); J. K. Glasbrenner, I. I. Mazin, H. O. Jeschke, P. J. Hirschfeld, R. M. Fernandes, and R. Valentí, Nat. Phys. **11**, 953 (2015); A. Baum, H. N. Ruiz, N. Lazarević, Y. Wang, T. Böhm *et al.*, Commun. Phys. **2**, 14 (2019).

Supplementary Material

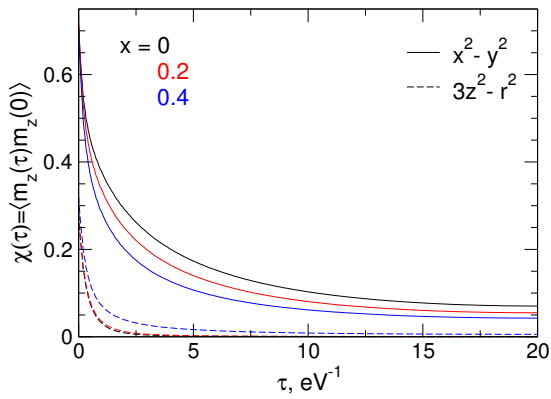


FIG. S1: Orbitally resolved local spin correlation functions $\chi(\tau) = \langle \hat{m}_z(\tau) \hat{m}_z(0) \rangle$ of Sr-doped NdNiO₂ as a function of hole doping Sr x calculated by DFT+DMFT at $T = 290$ K.

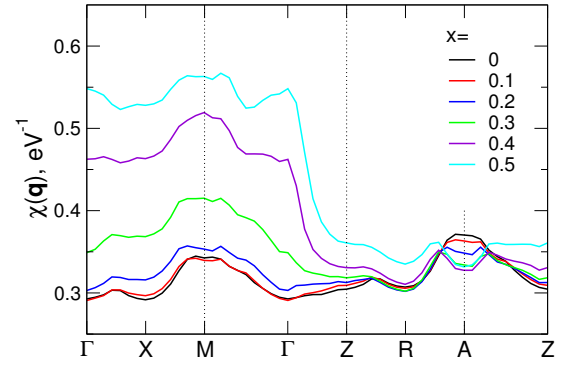


FIG. S2: Static spin susceptibility $\chi(\mathbf{q})$ of Sr-doped NdNiO₂ as a function of hole doping Sr x calculated by DFT+DMFT at $T = 290$ K.

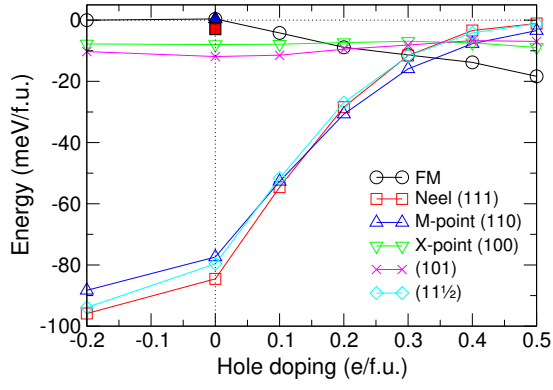


FIG. S3: Total energy difference $\Delta E = E_{\text{mag.}} - E_{\text{NM}}$ between the long-range magnetically ordered and non-magnetic states of NdNiO_2 as a function of hole doping calculated by DFT (empty symbols). Ferromagnetic (FM), Néel (111), C -type (110), (101) and single stripe (100), and staggered dimer ($11\frac{1}{2}$) states are shown. DFT+DMFT results for the total energy difference between the Néel and C -type AFM states and the paramagnetic state at $T = 290$ K are depicted by filled symbols.